nature geoscience

ARTICLES

https://doi.org/10.1038/s41561-021-00722-3

Global carbon dioxide efflux from rivers enhanced by high nocturnal emissions

Lluís Gómez-Gener[1,24] ✉, Gerard Rocher-Ros[2,24] ✉, Tom Battin[1], Matthew J. Cohen[3], Higo J. Dalmagro[4], Kerry J. Dinsmore[5], Travis W. Drake[6], Clément Duvert[7], Alex Enrich-Prast[8,9], Åsa Horgby[1], Mark S. Johnson[10,11], Lily Kirk[12], Fausto Machado-Silva[9], Nicholas S. Marzolf[13], Mollie J. McDowell[10,11], William H. McDowell[14], Heli Miettinen[15], Anne K. Ojala[16], Hannes Peter[1], Jukka Pumpanen[17], Lishan Ran[18], Diego A. Riveros-Iregui[19], Isaac R. Santos[20], Johan Six[6], Emily H. Stanley[21], Marcus B. Wallin[22], Shane A. White[23] and Ryan A. Sponseller[2]

Carbon dioxide (CO_2) emissions to the atmosphere from running waters are estimated to be four times greater than the total carbon (C) flux to the oceans. However, these fluxes remain poorly constrained because of substantial spatial and temporal variability in dissolved CO_2 concentrations. Using a global compilation of high-frequency CO_2 measurements, we demonstrate that nocturnal CO_2 emissions are on average 27% (0.9 gC m^{-2} d^{-1}) greater than those estimated from diurnal concentrations alone. Constraints on light availability due to canopy shading or water colour are the principal controls on observed diel (24 hour) variation, suggesting this nocturnal increase arises from daytime fixation of CO_2 by photosynthesis. Because current global estimates of CO_2 emissions to the atmosphere from running waters (0.65–1.8 PgC yr^{-1}) rely primarily on discrete measurements of dissolved CO_2 obtained during the day, they substantially underestimate the magnitude of this flux. Accounting for night-time CO_2 emissions may elevate global estimates from running waters to the atmosphere by 0.20–0.55 PgC yr^{-1}.

Carbon dioxide (CO_2) emission from inland waters to the atmosphere is a major flux in the global carbon (C) cycle, four-fold larger than the lateral C export to oceans[1]. Streams and rivers are hotspots for this flux, accounting for ~85% of inland water CO_2 emissions despite covering <20% of the freshwater surface area[2]. However, the magnitude of global CO_2 emissions from streams and rivers remains highly uncertain with estimates updated over the past decade from 0.6 to 3.48 PgC yr^{-1} (refs. [2,3]). This revision follows improvements in the spatial resolution for upscaling emissions[2,4], as well as new studies from previously underrepresented areas such as the Congo[5], Amazon[6,7] and global mountains[8]. Despite recent studies using continuous measurements to show large day–night changes in stream and river water CO_2 concentrations[9–13], the global importance of sub-daily variation on overall CO_2 emissions remains unexplored.

Diurnal cycles in solar radiation impose a well-known periodicity on stream biogeochemical processes, creating diel (that is, 24-hour periods) patterns for many solutes and gases, including nutrients, dissolved organic matter and dissolved oxygen (O_2)[14]. Indeed, diel variation in O_2 arising from photosynthetic activity is the signal from which whole-system metabolic fluxes are estimated[15]. Photosynthetic production of O_2 is stoichiometrically linked to the daytime assimilation of dissolved inorganic carbon (principally dissolved CO_2), lowering CO_2 concentrations during the day. The resulting diel variation, with higher night-time CO_2 concentrations when respiration reactions dominate, implies increased emissions at night. Despite the obvious connection between photosynthesis and CO_2 consumption, the implications for total aquatic CO_2 emissions have been neglected, most likely due to the lack of sub-daily measurements of CO_2 in water[16]. Other processes can also vary at

[1]Stream Biofilm and Ecosystem Research Laboratory, School of Architecture, Civil and Environmental Engineering, Ecole Polytechnique Fédérale de Lausanne, Lausanne, Switzerland. [2]Department of Ecology and Environmental Science, Umeå University, Umeå, Sweden. [3]School of Forest Resources and Conservation, University of Florida, Gainesville, FL, USA. [4]University of Cuiabá, Cuiabá, Brazil. [5]Centre for Ecology and Hydrology, Bush Estate, Penicuik, UK. [6]Department of Environmental Systems Science, ETH Zürich, Zürich, Switzerland. [7]Research Institute for the Environment and Livelihoods, Charles Darwin University, Darwin, Northern Territory, Australia. [8]Biogas Research Center and Department of Thematic Studies–Environmental Change, Linköping University, Linköping, Sweden. [9]Post-Graduate Program in Geosciences (Environmental Geochemistry), Chemistry Institute, Fluminense Federal University, Niterói, Brazil. [10]Institute for Resources, Environment and Sustainability, University of British Columbia, Vancouver, British Columbia, Canada. [11]Department of Earth, Ocean and Atmospheric Sciences, University of British Columbia, Vancouver, British Columbia, Canada. [12]School of Natural Resources and Environment, University of Florida, Gainesville, FL, USA. [13]Department of Forestry and Environmental Resources, North Carolina State University, Raleigh, NC, USA. [14]Department of Natural Resources and the Environment, University of New Hampshire, Durham, NH, USA. [15]Department of Forest Ecology and Management, Swedish University of Agricultural Sciences, Umeå, Sweden. [16]Faculty of Biological and Environmental Sciences, Ecosystems and Environment Research Programme, University of Helsinki, Helsinki, Finland. [17]Department of Environmental and Biological Sciences, University of Eastern Finland, Kuopio, Finland. [18]Department of Geography, The University of Hong Kong, Pokfulam, Hong Kong. [19]Department of Geography, University of North Carolina at Chapel Hill, Chapel Hill, NC, USA. [20]Department of Marine Sciences, University of Gothenburg, Gothenburg, Sweden. [21]Center for Limnology, University of Wisconsin-Madison, Madison, WI, USA. [22]Department of Aquatic Sciences and Assessment, Swedish University of Agricultural Sciences, Uppsala, Sweden. [23]National Marine Science Centre, Southern Cross University, Coffs Harbour, New South Wales, Australia. [24]These authors contributed equally: Lluís Gómez-Gener, Gerard Rocher-Ros. ✉e-mail: gomez.gener87@gmail.com; gerard.rocher@umu.se

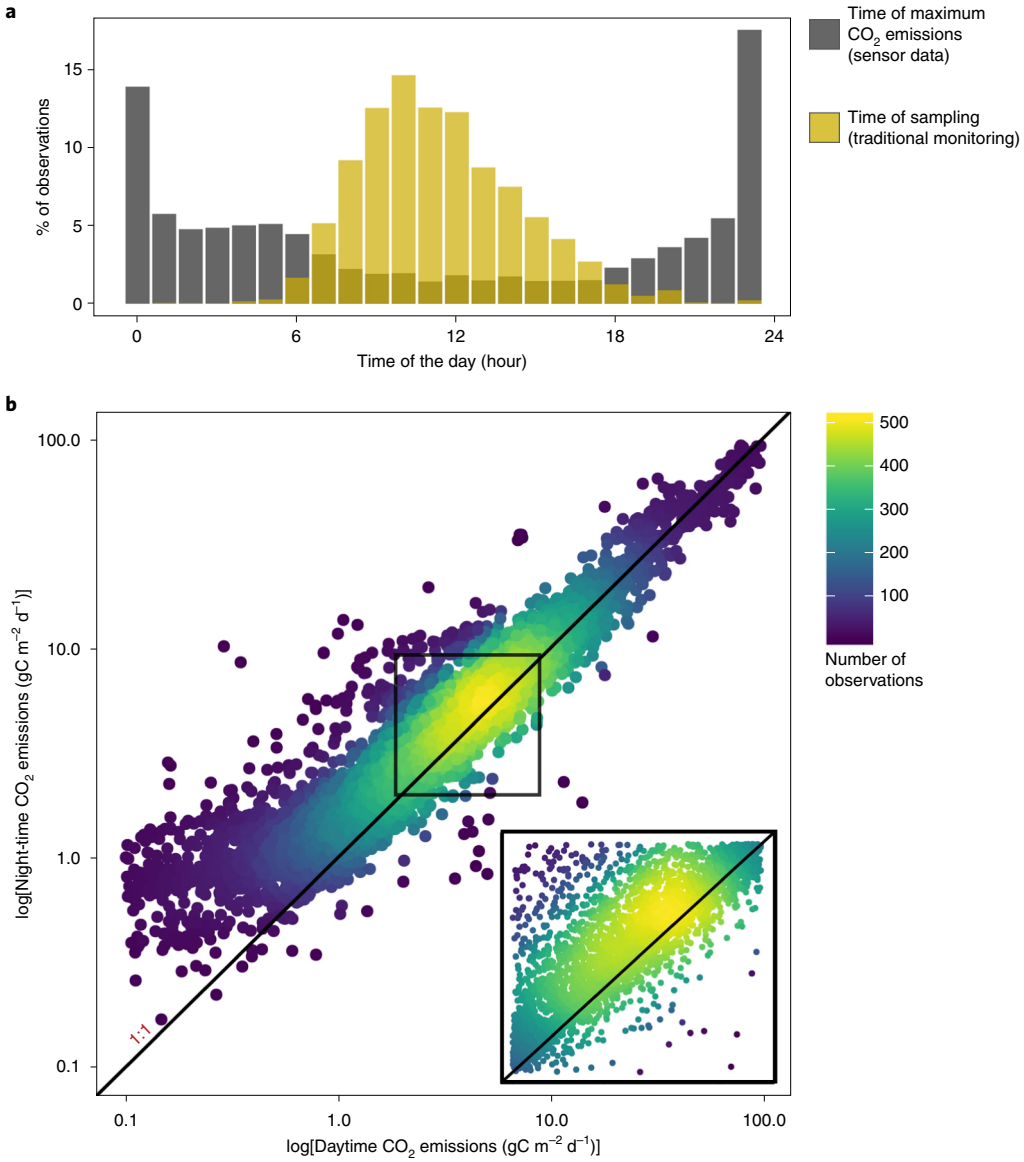

Fig. 1 | Magnitude and bias of diel variation in CO_2 emission fluxes from global streams. a, Distribution of manual sampling times in the GLORICH database[20] together with the time of maximum CO_2 emission fluxes from sensor data (this study). **b**, Relationship between the median day and night CO_2 emission flux (gC m^{-2} d^{-1}) for all study sites and days. The black 1:1 line indicates that 75.2% of daily observations exhibit enhanced nocturnal emissions. The inset illustrates the distribution of observations in the densest region of the graph.

sub-daily timescales and could thus similarly drive diel changes in CO_2 emissions from streams, including interactions with the carbonate system[17], photochemical oxidation of organic matter[18] and diel changes in discharge and subsequently lateral CO_2 inputs from terrestrial environments[19]. Regardless of the driving forces, the overall magnitude, direction and importance of diel changes in CO_2 emissions remain largely unknown at a global scale.

Current global estimates of CO_2 emissions from running waters[2,4] rely almost exclusively on manually collected samples that fail to incorporate sub-daily variability. Here, we assess whether widespread reliance on discrete daytime sampling creates a strong temporal bias that underestimates CO_2 emissions from running waters. We use the most widely used GLObal RIver CHemistry database (GLORICH; ref. [20]) and leverage recent technological advances in continuous, sensor-based dissolved CO_2 monitoring[16] to ask if this sampling bias is concurrent with consistent day–night differences in CO_2 emissions. We compiled high-resolution CO_2 time series representing a total of 57 years of continuous data from 66 streams worldwide (Extended Data Fig. 1a; Supplementary Table 1), spanning a wide range of drainage sizes (Extended Data Fig. 1b), climate conditions, land cover and stream physicochemical properties (Supplementary Table 2). We evaluated the generality of diurnal stream CO_2 variation, quantified the importance of these signals for CO_2 emissions and identified the main landscape factors that control diurnal variation. Finally, we evaluated the potential bias in global estimates that arises from neglecting nocturnal CO_2 emissions.

Results and Discussion

Magnitude and bias of diel changes in CO_2 emissions. Water samples compiled in the GLORICH database[20] were primarily taken during the day, with 90% of observations between 08:10 and 15:55 and a median sampling time of 11:25 (Fig. 1a). Comparing this time window of manual sampling with sensor data synthesized in this study, we found that only 10% of days had maximum CO_2 emissions

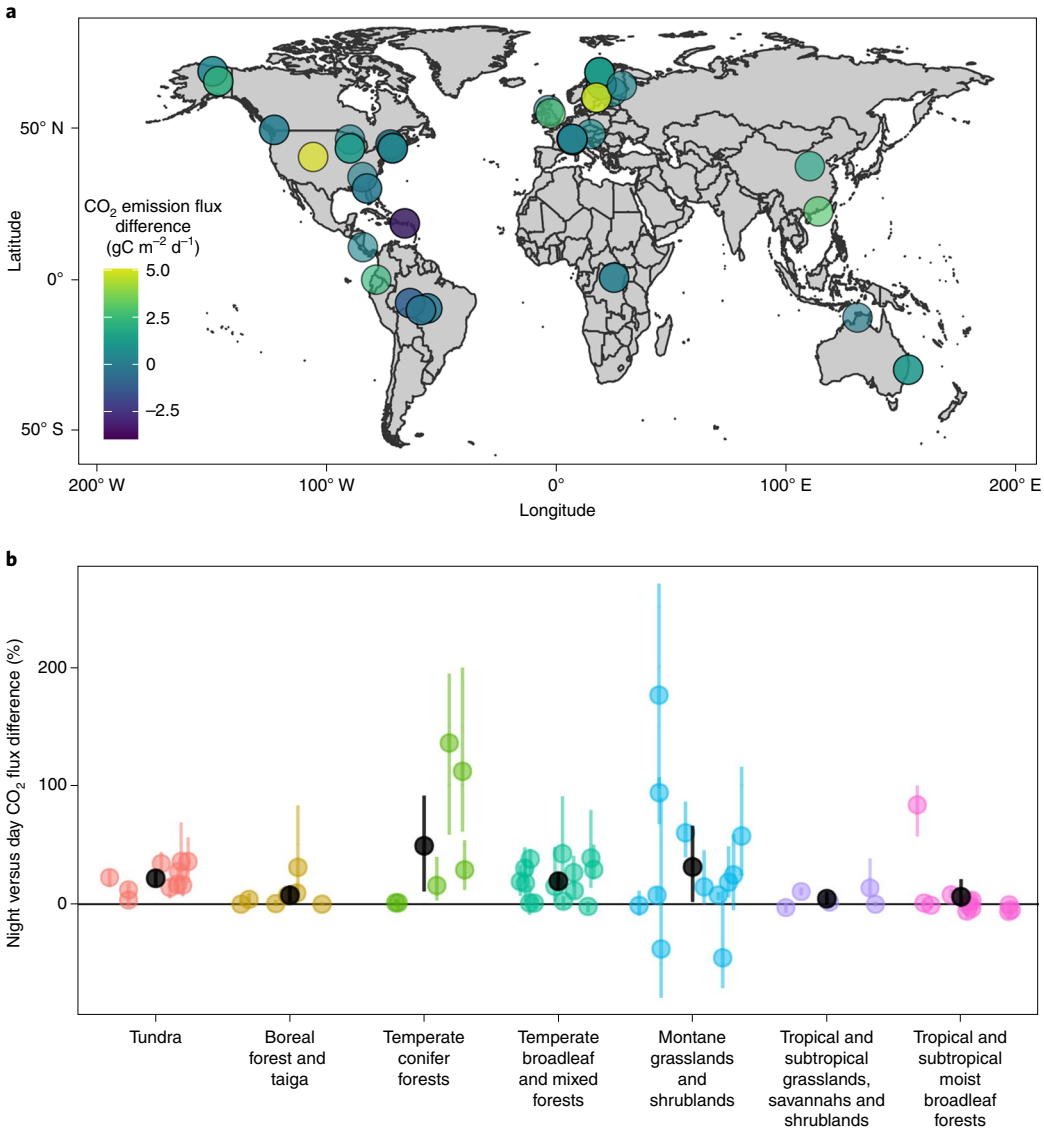

Fig. 2 | Geographical distribution of diel variation in stream CO_2 emission fluxes. a, Global patterns of night versus day differences in CO_2 emission fluxes averaged by stream (in gC m^{-2} d^{-1}; Supplementary Table 3 contains a detailed summary). **b**, Night–day differences in CO_2 emission fluxes averaged by stream and grouped by biome (in per cent; Supplementary Table 3 contains a more detailed summary). The black point and bar represent the mean and 95% bootstrapped confidence interval for each biome.

within these hours, and there was a consistent pattern of higher emission rates at night than during the day (Fig. 1b). Nocturnal emission rates were on average 27% greater than daytime rates across all sites, with differences ranging from −12 to 193% (Supplementary Table 3). This overall pattern was globally consistent, with 56 of 66 (85%) of sites showing higher average nocturnal CO_2 emission rates (Fig. 2a and Supplementary Table 3). However, the observed ranges in diel change varied among biomes (Fig. 2b). Specifically, streams with the largest diel change in emissions drained temperate forests, followed by montane grasslands; yet these biomes also had the largest internal variation. We observed generally smaller diel changes and less internal variability for boreal and tropical/subtropical systems. Despite such differences, the large variation observed within most biomes suggests that controls on diel CO_2 emissions operate at finer spatial scales[10]. Further, because the GLORICH database, the foundation of current global estimates of CO_2 emissions from inland waters[2], relies primarily on discrete samples with a strong daytime sampling bias, the geographically widespread diel variation in CO_2 emissions introduces a systematic and potentially large error in estimates of aggregate flux rates.

Drivers of diel changes in CO_2 emissions. Diel patterns in stream CO_2 emissions result from a dynamic interplay between biogeochemical and hydrological processes. These diel drivers include aquatic primary production[10,12], biological[21] and photolytic oxidation of organic C (ref. [18]) and terrestrial import of CO_2 from soil respiration and mineral weathering[19]. Additionally, diel changes in water temperature can affect CO_2 emissions through its effect on the physical exchange rate between air and water (k_{CO_2})[22]. An initial exploration of our continuous data suggests that aquatic processes generate considerable temporal variation in the magnitude of diel variation in emissions (Fig. 3). Specifically, for sites with annual records, the largest diel amplitudes were consistently observed during summer and in open-canopy reaches (median = 0.76 gC m^{-2} d^{-1}). Markedly reduced amplitudes were observed in streams with closed canopies (median = 0.09 gC m^{-2} d^{-1}), while intermediate amplitudes

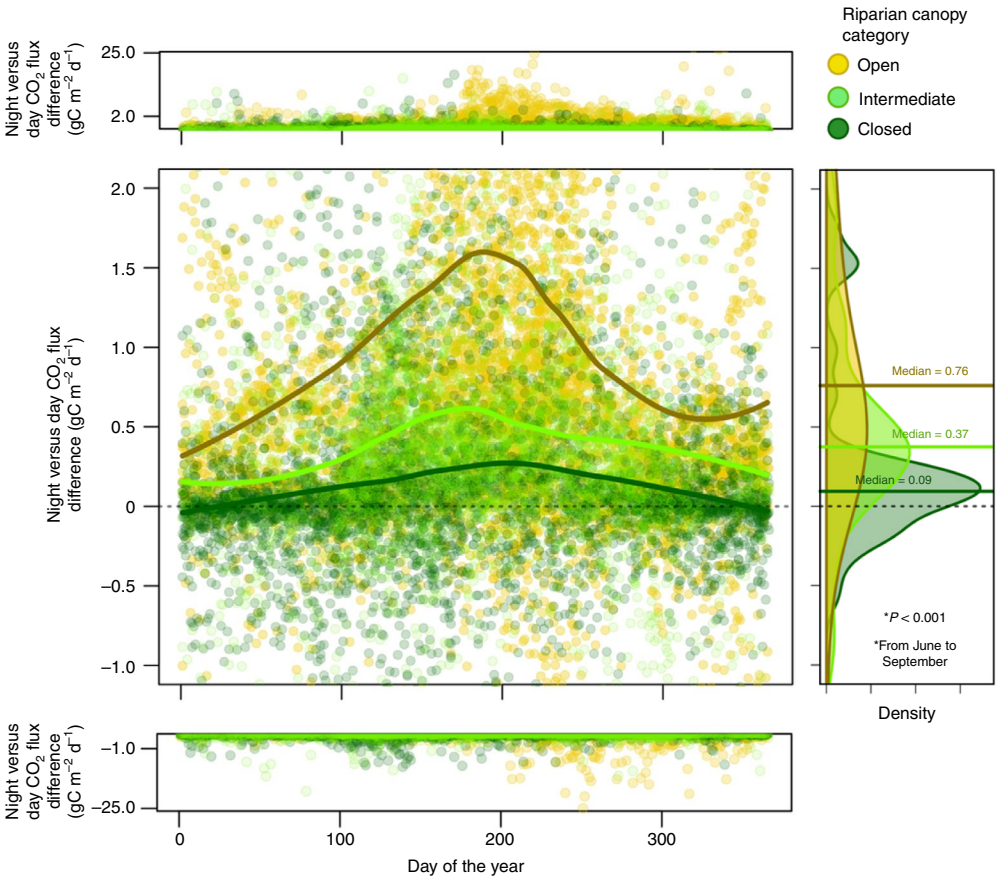

Fig. 3 | Seasonal pattern of diel changes in CO_2 emission fluxes from streams. Seasonal variation in the night versus day difference of CO_2 emission fluxes (gC m^{-2} d^{-1}) grouped by riparian canopy-cover category (open, yellow; intermediate, light green; closed; dark green; 33, 16 and 17 sites and 5,780, 3,814 and 5,130 daily observations, respectively; see Methods and Supplementary Table 2). The coloured solid lines are locally weighted (loess) regression model fits for a visual interpretation. Panels at the top and bottom show extreme positive and negative values, respectively (note change in scaling). Density plots show distributions of night versus day differences of CO_2 emission fluxes (gC m^{-2} d^{-1}) grouped by canopy cover during summer. Differences between canopy levels were evaluated using the non-parametric Kruskal–Wallis test.

were evident at partially covered sites (median = 0.37 gC m^{-2} d^{-1}). Overall, these observations are consistent with greater levels of daytime CO_2 uptake in open-canopy streams during summer, when warm temperatures and greater incident light[23,24] support elevated rates of photosynthesis[10]. By contrast, wintertime diel changes in stream CO_2 emissions were more similar across canopy-cover categories, suggesting reduced aquatic photosynthesis.

We used structural equation modelling (SEM) to further resolve factors and causal combinations that underpin variation in summertime diel emissions, the time period for which we have the most complete dataset (Supplementary Fig. 1; Supplementary Table 1). Our structural model consisted of two levels of factor interaction, or metamodels (Methods contains a more detailed description of the SEM). First, we considered whether diel CO_2 emission patterns arise from parallel variation in k_{CO_2} and CO_2 partial pressure (p_{CO_2}), the two main factors determining aquatic CO_2 emissions[25]. The results from the SEM at this first level ($R^2 = 0.43$; Extended Data Fig. 2 and Supplementary Table 4) suggest that diel variation in CO_2 emissions was mostly driven by variation in p_{CO_2} (standardized path coefficient, $\beta = 0.65$), whereas k_{CO_2} exerted a minor influence ($\beta = 0.02$). Second, we used SEM to identify statistically significant relationships between environmental variables and diel changes in p_{CO_2}. This second SEM model ($R^2 = 0.46$; Extended Data Fig. 2 and Supplementary Table 4) indicated that stream canopy cover ($\beta = -0.58$) was the primary driver of diel variation of p_{CO_2}. Together with the observed seasonal patterns (Fig. 3), our model supports the hypothesis that riparian canopy cover drives diel p_{CO_2} variation by regulating the amount of light reaching the stream surface and, in turn, daytime rates of stream autotrophic CO_2 uptake[15,26,27].

Diel patterns in stream CO_2 emissions not only varied seasonally but also spatially, increasing with channel size (Fig. 4a). In larger river systems, terrestrial shading is reduced, increasing the light available for primary producers[23], which ultimately explains the general increase in gross primary production (GPP) with channel size[28,29]. However, larger rivers with open canopies in our dataset did not necessarily exhibit large diel changes in CO_2 emissions (Fig. 4b). The variability in diel CO_2 amplitudes among these larger rivers probably arises from differences in light attenuation in the water column, linked to high concentrations of dissolved organic matter (DOM) or suspended sediments that inhibit GPP[30] (Fig. 4c and Extended Data Fig. 3). As such, light attenuation, either by canopy cover along small streams or by water colour, turbidity and/or depth for larger river systems[31], dictates the magnitude of diel variation in CO_2 emissions along river continua. We further explored the influences of water colour at five subtropical Florida sites spanning a large range in concentration of dissolved organic carbon (DOC; 1.0–43.4 mg l^{-1}) and ecosystem size (9–66 m^3 s^{-1} median discharge), and for which we have high-frequency CO_2 and fluorescent DOM (fDOM) measurements. These data confirm that diel changes in CO_2 emissions are suppressed above ~70 ppb of fDOM (corresponding to ~20 mg l^{-1} DOC), even when incident light is relatively high (Fig. 4d). Despite this potential influence of water colour, more than

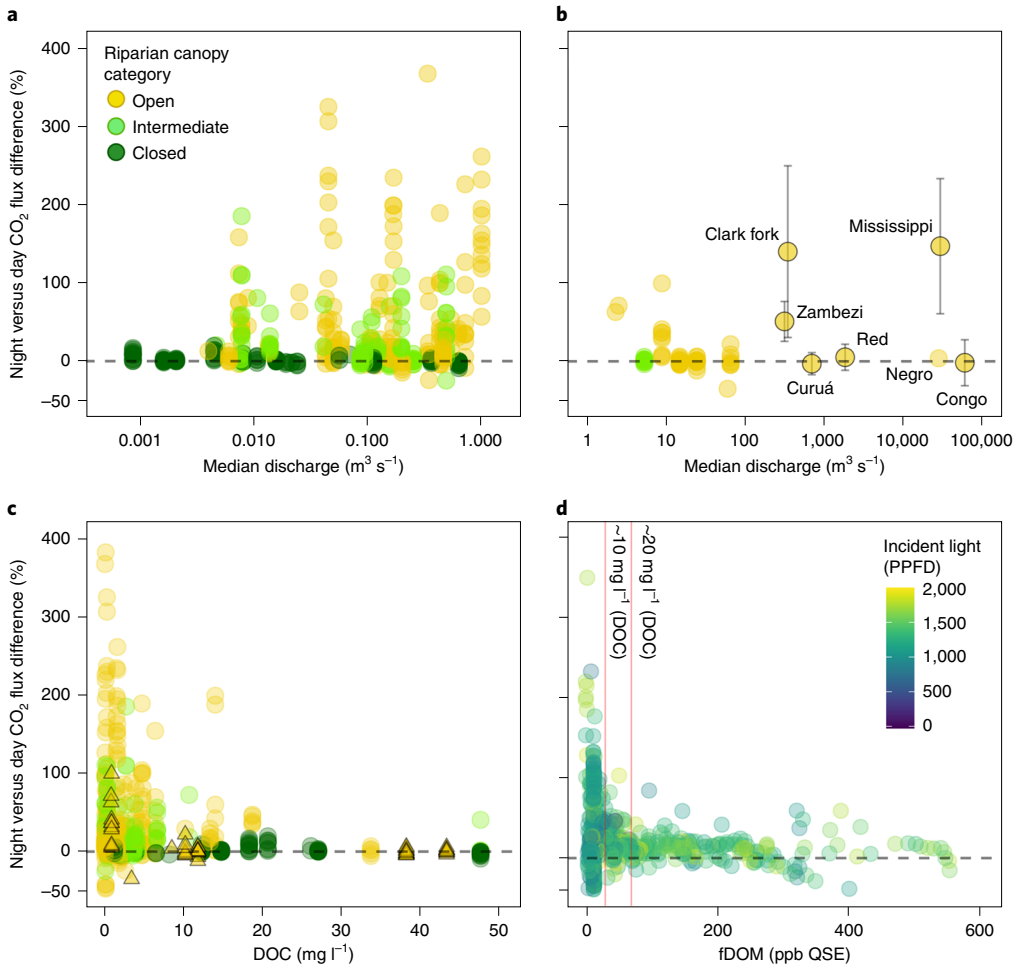

Fig. 4 | Night versus day differences in CO_2 emission fluxes along the river size and colour continuum. a,**b**, Relationship between the night–day difference of CO_2 emission fluxes (%) and the median annual discharge (m^3 s^{-1}) for streams (**a**) (watercourses with median discharge equal or below 1.5 m^3 s^{-1}, catchment area equal or below 246 km^2, Extended Data Fig. 1), coloured by canopy-cover category, and rivers (**b**) (watercourses with median discharge above 1.5 m^3 s^{-1}, catchment area above 246 km^2, Extended Data Fig. 1). Each point represents a monthly average for each site, except for data from the six additional rivers (circles with grey error bars) obtained from the literature (Supplementary Table 5). **c**, Relationship between the night–day difference in CO_2 emission fluxes (%) and the mean DOC concentration (mg l^{-1}) for streams (circles) and rivers (triangles), coloured by canopy-cover category (Extended Data Fig. 1). **d**, Relationship between the daily night–day difference of CO_2 emission fluxes (%) and the daily fDOM concentration (ppb quinine sulfate equivalent; QSE) for the five rivers in Florida with high-frequency water-colour data (Extended Data Fig. 1 and Supplementary Table 5), coloured by incident light (as photosynthetic photon flux density, PPFD).

95% of the sites in the GLORICH database have below 20 mg l^{-1} of DOC (Extended Data Fig. 4), and thus water colour as a constraint on diel CO_2 patterns is probably not operating for most of the monitoring sites from which global estimates of river CO_2 emissions are currently derived.

The controls on diel variation in CO_2 emissions exerted by either canopy cover or water colour do not follow obvious geographical patterns (Fig. 2b). However, the probability that one or both constraints operate is probably biome-specific, which may aid in predictions of which regions of Earth are more prone to strong bias in upscaling. For example, boreal and tropical regions are typically characterized by forests with dense canopies and can support aquatic systems with dark, DOC-rich waters[32,33] (Extended Data Fig. 5). Indeed, for these biomes we observed, on average, a lower diel change in CO_2 emissions (Fig. 2b). In this context, observations from the subtropical Florida sites (Fig. 4d) probably provide insight into the expected dynamics for dark-water systems elsewhere, including tropical rivers that are otherwise poorly represented in our analysis. For some biomes (for example, montane grasslands and tundra), limited canopy cover and low catchment DOC production make light constraints on aquatic GPP and diel CO_2 emissions less likely, while in other settings (for example, human-dominated landscapes) land-cover change and nutrient enrichment can amplify diel CO_2 variation by stimulating rates of algal photosynthesis[30]. Overall, we suggest that future efforts to resolve the fine-scale spatial patterns of canopy cover and DOM in running waters are needed to further refine our understanding of aquatic GPP and its implications for CO_2 emissions.

Implications for global CO_2 emissions from running waters. Our analysis reveals important consequences for global estimates of CO_2 emissions from running waters: (1) current estimates based on discrete samples are heavily biased towards daytime, (2) CO_2 emission rates are consistently higher at night due to variations in aquatic p_{CO_2} and (3) this pattern is primarily driven by light availability and is widespread across biomes and along river continua. To quantify this underestimation of CO_2 emissions, we compare the measured total emissions for each site with the emissions estimated considering only the CO_2 concentrations observed between 10:00 and 14:00 (the interquartile sampling time in the GLORICH database; Fig. 1a). Across all 66 sites, CO_2 emissions integrated over a full day were

35% higher than those based on samples taken at midday (range: −7–369%; 95% confidence interval: 14–47%). Based on the two current global estimates of stream CO_2 emissions of 0.6–1.8 PgC yr^{-1} (refs. [2,4]) and our estimate of this proportional bias, we suggest that an additional 0.20–0.55 PgC yr^{-1} of CO_2 may be emitted from streams globally (95% confidence interval: 0.09–0.30 and 0.25–0.84, respectively). However, given that the current global estimates of C emissions from running waters are still highly uncertain and remain unbalanced by global C budgets[34], this additional flux of CO_2 should be taken with caution as global estimates continue to be refined.

We also emphasize other important sources of uncertainty in the global estimates of emissions from running waters, upon which our calculations are based. For example, current estimates[2,4] are derived from indirect determinations of surface water CO_2 from alkalinity and pH, which can be highly biased[35,36]. Further, the notoriously variable nature of hydrodynamic factors that influence CO_2 emissions cannot be easily aggregated at large spatial scales[37,38]. It is also problematic that current estimates are biased towards observations from mid-to-high latitudes, even though underrepresented tropical systems may be key contributors to global CO_2 emissions[5,39]. Our study, while covering most biomes and spanning large gradients in canopy cover and water colour, also suffers from this bias. Despite this, our assessment provides a compilation of direct, high-frequency measurements of CO_2 in flowing waters from across the globe that helps refine global estimates of CO_2 emissions from inland waters. While the magnitude of this global estimate will be improved with further measurements, the broad consistency and strength of the patterns observed here suggest that nocturnal emissions of CO_2 from streams and rivers are a major unaccounted flux in the global C cycle.

Online content

Any methods, additional references, Nature Research reporting summaries, source data, extended data, supplementary information, acknowledgements, peer review information; details of author contributions and competing interests; and statements of data and code availability are available at https://doi.org/10.1038/s41561-021-00722-3.

Received: 26 August 2020; Accepted: 25 February 2021;
Published online: 15 April 2021

References

1. Cole, J. J. et al. Plumbing the global carbon cycle: integrating inland waters into the terrestrial carbon budget. *Ecosystems* **10**, 171–185 (2007).
2. Raymond, P. A. et al. Global carbon dioxide emissions from inland waters. *Nature* **503**, 355–359 (2013).
3. Drake, T. W., Raymond, P. A. & Spencer, R. G. M. Terrestrial carbon inputs to inland waters: a current synthesis of estimates and uncertainty. *Limnol. Oceanogr. Lett.* https://doi.org/10.1002/lol2/.10055 (2017).
4. Lauerwald, R., Laruelle, G. G., Hartmann, J., Ciais, P. & Regnier, P. A. G. Spatial patterns in CO_2 evasion from the global river network. *Global Biogeochem. Cycles* **29**, 534–554 (2015).
5. Borges, A. V. et al. Globally significant greenhouse-gas emissions from African inland waters. *Nat. Geosci.* **8**, 637–642 (2015).
6. Sawakuchi, H. O. et al. Carbon dioxide emissions along the lower Amazon River. *Front. Mar. Sci.* **4**, 76 (2017).
7. Hastie, A., Lauerwald, R., Ciais, P. & Regnier, P. Aquatic carbon fluxes dampen the overall variation of net ecosystem productivity in the Amazon basin: an analysis of the interannual variability in the boundless carbon cycle. *Glob. Change Biol.* **25**, 2094–2111 (2019).
8. Horgby, Å. et al. Unexpected large evasion fluxes of carbon dioxide from turbulent streams draining the world's mountains. *Nat. Commun.* **10**, 4888 (2019).
9. Peter, H. et al. Scales and drivers of temporal p_{CO_2} dynamics in an Alpine stream. *J. Geophys. Res. Biogeosci.* **119**, 1078–1091 (2014).
10. Rocher-Ros, G., Sponseller, R. A., Bergstr, A., Myrstener, M. & Giesler, R. Stream metabolism controls diel patterns and evasion of CO_2 in Arctic streams. *Glob. Change Biol.* https://doi.org/10.1111/gcb.14895 (2020).
11. Wallin, M. B., Audet, J., Peacock, M., Sahlée, E. & Winterdahl, M. Carbon dioxide dynamics in an agricultural headwater stream driven by hydrology and primary production. *Biogeosciences* **17**, 2487–2498 (2020).
12. Crawford, J. T., Stanley, E. H., Dornblaser, M. M. & Striegl, R. G. CO_2 time series patterns in contrasting headwater streams of North America. *Aquat. Sci.* **79**, 473–486 (2017).
13. Reiman, J. & Xu, Y. J. Diel variability of p_{CO_2} and CO_2 outgassing from the lower Mississippi River: implications for riverine CO_2 outgassing estimation. *Water* **11**, 43 (2018).
14. Hensley, R. T. & Cohen, M. J. On the emergence of diel solute signals in flowing waters. *Water Resour. Res.* **52**, 759–772 (2016).
15. Odum, H. T. Primary production in flowing waters. *Limnol. Oceanogr.* **1**, 102–117 (1955).
16. Johnson, M. S. et al. Direct and continuous measurement of dissolved carbon dioxide in freshwater aquatic systems—method and applications. *Ecohydrology* **3**, 68–78 (2010).
17. Stets, E. G. et al. Carbonate buffering and metabolic controls on carbon dioxide in rivers. *Global Biogeochem. Cycles* **31**, 663–677 (2017).
18. Cory, R. M., Ward, C. P., Crump, B. C. & Kling, G. W. Sunlight controls water column processing of carbon in Arctic fresh waters. *Science* **345**, 925–928 (2014).
19. Riml, J., Campeau, A., Bishop, K. & Wallin, M. B. Spectral decomposition reveals new perspectives on CO_2 concentration patterns and soil–stream linkages. *J. Geophys. Res. Biogeosci.* https://doi.org/10.1029/2018JG004981 (2019).
20. Hartmann, J., Lauerwald, R. & Moosdorf, N. A brief overview of the GLObal RIver CHemistry Database, GLORICH. *Procedia Earth Planet. Sci.* **10**, 23–27 (2014).
21. Hotchkiss, E. R. et al. Sources of and processes controlling CO_2 emissions change with the size of streams and rivers. *Nat. Geosci.* **8**, 696–699 (2015).
22. Demars, B. O. L. & Manson, J. R. Temperature dependence of stream aeration coefficients and the effect of water turbulence: a critical review. *Water Res.* **47**, 1–15 (2013).
23. Koenig, L. E. et al. Emergent productivity regimes of river networks. *Limnol. Oceanogr.* **4**, 173–181 (2019).
24. Bernhardt, E. S. et al. The metabolic regimes of flowing waters. *Limnol. Oceanogr.* **63**, S99–S118 (2018).
25. Raymond, P. A. et al. Scaling the gas transfer velocity and hydraulic geometry in streams and small rivers. *Limnol. Oceanogr. Fluids Environ.* **2**, 41–53 (2012).
26. Mulholland, P. J. et al. Inter-biome comparison of factors controlling stream metabolism. *Freshw. Biol.* **46**, 1503–1517 (2001).
27. Roberts, B. J., Mulholland, P. J. & Hill, W. R. Multiple scales of temporal variability in ecosystem metabolism rates: results from 2 years of continuous monitoring in a forested headwater stream. *Ecosystems* **10**, 588–606 (2007).
28. Vanote, R. L., Minshall, W. G., Cummins, K. W., Sedell, J. R. & Cushing, C. E. The river continuum concept. *Can. J. Fish. Aquat. Sci.* **37**, 130–137 (1980).
29. Finlay, J. C. Stream size and human influences on ecosystem production in river networks. *Ecosphere* **2**, art87 (2011).
30. Kirk, L., Hensley, R. T., Savoy, P., Heffernan, J. B. & Cohen, M. J. Estimating benthic light regimes improves predictions of primary production and constrains light-use efficiency in streams and rivers. *Ecosystems* https://doi.org/10.1007/s10021-020-00552-1 (2020).
31. Julian, J. P., Doyle, M. W., Powers, S. M., Stanley, E. H. & Riggsbee, J. A. Optical water quality in rivers. *Water Resour. Res.* **44**, W10411 (2008).
32. Aitkenhead, J. A. & McDowell, W. H. Soil C:N ratio as a predictor of annual riverine DOC flux at local and global scales. *Global Biogeochem. Cycles* **14**, 127–138 (2000).
33. Harrison, J. A., Caraco, N. & Seitzinger, S. P. Global patterns and sources of dissolved organic matter export to the coastal zone: results from a spatially explicit, global model. *Global Biogeochem. Cycles* **19**, GB4S04 (2005).
34. Friedlingstein, P. et al. Global carbon budget 2019. *Earth Syst. Sci. Data* **11**, 1783–1838 (2019).
35. Liu, S., Butman, D. E. & Raymond, P. A. Evaluating CO_2 calculation error from organic alkalinity and pH measurement error in low ionic strength freshwaters. *Limnol. Oceanogr. Methods* **18**, 606–622 (2020).
36. Abril, G. et al. Technical Note: Large overestimation of p_{CO_2} calculated from pH and alkalinity in acidic, organic-rich freshwaters. *Biogeosciences* **12**, 67–78 (2015).
37. Duvert, C., Butman, D. E., Marx, A., Ribolzi, O. & Hutley, L. B. CO_2 evasion along streams driven by groundwater inputs and geomorphic controls. *Nat. Geosci.* **11**, 813–818 (2018).
38. Rocher-Ros, G., Sponseller, R. A., Lidberg, W., Mörth, C. & Giesler, R. Landscape process domains drive patterns of CO_2 evasion from river networks. *Limnol. Oceanogr. Lett.* https://doi.org/10.1002/lol2.10108 (2019).
39. Richey, J. E., Melack, J. M., Aufdenkampe, A. K., Ballester, V. M. & Hess, L. L. Outgassing from Amazonian rivers and wetlands as a large tropical source of atmospheric CO_2. *Nature* **416**, 617–620 (2002).

Methods

Study sites and data acquisition. We compiled high-frequency dissolved CO_2 time series (median temporal resolution = 39 minutes; range 5 to 180 minutes) over at least 8 days (median time series duration = 317 days; range 8 to 1,553 days) from 66 headwater streams worldwide (Fig. 2a; Supplementary Table 1). We used median annual discharge (which covaried with catchment surface area; Extended Data Fig. 1) as a criterion to select streams (that is, median annual discharge equal or below 1.5 $m^3 s^{-1}$, catchment area <246 km^2; orders 1 to 3 (ref. [40])). Selected streams come from multiple biomes, including tropical forests and savannah, temperate forests, boreal forest and taiga, Arctic tundra, high-mountain forests and grasslands, and, accordingly, a wide range of climatic and biogeographic conditions (Supplementary Table 2). Sites also encompass a variety of catchment features (for example, land cover, altitude and surface area) and reach-scale hydrological, morphometric and physicochemical properties (Supplementary Table 2).

High-frequency CO_2 measurements were obtained from a variety of sources, including unpublished time series, monitoring network platforms (for example, StreamPULSE, https://data.streampulse.org/) and literature datasets[8–12,16,41–43] (Supplementary Table 1). In all cases, CO_2 was measured using in-situ automated sensors connected to data loggers (Supplementary Table 1). The measurement accuracy of the CO_2 sensors ranged from ±1% to ±3%. In addition, water temperature (in all streams) and discharge (in 57 of 66 streams; continuous discharge derived from water depth sensor data) were also measured at the same frequency as CO_2 using in-situ automated sensors. Additional datasets[13,44–47] were included in this study but not directly used in the main analysis (used only to construct Fig. 4b-d) because they were either from considerably larger rivers (median discharge above 1.5 $m^3 s^{-1}$, Extended Data Fig. 1), based on high-frequency but short-term deployments (<8 days) and/or based in discrete (not high-frequency) measurements of CO_2 emissions (details for these observations are found in Supplementary Table 5).

Time series processing. We standardized each time series to an hourly time step by resampling higher frequency measurements and interpolating lower frequency measurements. We also normalized CO_2 concentrations to CO_2 partial pressures (p_{CO_2}, ppm), corrected for temperature and pressure variation and removed obvious measurement errors (p_{CO_2} < 0 ppm. In total, the high-frequency dataset used for analysis included 457,637 hourly CO_2, temperature and discharge observations. Of the time series, 32 covered at least one complete year, 7 covered more than 200 days and the remaining 27 covered between 8 and 198 days, mostly during the summer (Supplementary Fig. 1).

Compilation of ancillary variables. Stream-reach canopy cover was determined by visually inspecting orthophotos of the study sites. High-resolution orthophotos from Google Earth imagery were downloaded at the highest resolution possible using the ggmap package (version 3.0.0) in R and classified in three categories of 'open' (0), 'intermediate' (1) or 'closed' canopy (2). The 'open' category was selected when it was possible to see the full extent of the stream channel, 'intermediate' when some parts of the stream were visible and 'closed' when it was not possible to detect the presence of a stream based on an orthophoto (Supplementary Fig. 2).

Stream channel slope was determined by measuring the difference in elevation between the sampling location and 300 m upstream following the channel. To do this, we downloaded digital elevation models (DEMs) at resolutions ranging between 1.9 and 14 m (depending on the location) using the elevatr package (version 0.2.0) in R. Then, for each site a raster of the flow-accumulation was produced using the whitebox package (version 0.5.0) in R, after initially breaching depressions for hydrological correctness. By combining the flow-accumulation raster with the DEM, we extracted the stream path and the elevation at the site and 300 m upstream (in QGIS 3.2.1).

Land cover was determined using the Global Land Cover Maps (100 m resolution; Copernicus Global Land Service) and the catchment boundaries delineated using high-resolution DEMs (2 × 2 m) in QGIS (version 3.2.1). Biome classifications were performed according to Olson et al.[48].

Mean annual concentrations (not flow-weighted) of DOC, nitrate (NO_3^-), ammonium (NH_4^+), pH and conductivity for the study streams were obtained from unpublished sources or extracted from the literature. Mean annual stream discharge and water temperature were computed from continuous time series.

Determination of CO_2 emissions. We estimated CO_2 emissions as the product of the gas transfer velocity (k_{CO_2}) and the concentration of dissolved CO_2 relative to atmospheric equilibrium[25]. A standardized gas transfer velocity (k_{600}) was obtained on the basis of the stream energy dissipation (eD)[49], defined as the product of channel slope (S; m m^{-1}), water velocity (V; m s^{-1}) and acceleration due to gravity (g; 9.8 m s^{-2}). We then calculated k_{600} as $k_{600} = e^{(3.1+0.35\times\log(eD))}$ for eD < 0.02 $m^2 s^{-3}$; and as $k_{600} = e^{(6.43+1.18\times\log(eD))}$ for eD > 0.02 $m^2 s^{-3}$. Water velocity was modelled using a power-law relationship with discharge[25]; in 4 streams discharge data were not available and we used a constant velocity of 0.2 m s^{-1}, the average velocity of the other sites. The k_{600} was converted to a gas- and temperature-specific gas transfer velocity k_{CO_2}, using the temperature-dependent Schmidt numbers for CO_2 (ref. [25]). Potential day–night differences in gas exchange required separate night and day k_{CO_2} calculations with time-of-day-specific velocity and temperature values. The CO_2 disequilibrium relative to the atmosphere was calculated as the difference in water and air p_{CO_2},converted to molar CO_2 concentrations using the temperature-specific Henry's constant. Atmospheric p_{CO_2} was assigned monthly to each site from the global average measured by the National Oceanic and Atmospheric Administration's Global Monitoring Laboratory (https://www.esrl.noaa.gov/gmd/ccgg/trends/global.html), which contains measurements between 2007 to 2020 that align spatially with our study. We assessed the importance of sub-daily changes in atmospheric concentrations by examining atmospheric measurements of p_{CO_2} from 14 streams and 77 ecosystem flux towers globally. We concluded that day–night changes in atmospheric p_{CO_2} are small and inconsistent, and therefore poorly constrained for extrapolation to other stream sites (section 1 in the Supplementary Information).

Finally, to assess whether a daytime sampling bias exists, we determined the distribution of sampling times in the GLORICH database[20]. From the database, we filtered all sampling occasions where both CO_2 (calculated from alkalinity and pH) and the time of sampling were available (n = 733,977 occasions from 8,520 locations), and then extracted summary statistics such as the median, 90% range and the interquartile range to compare with sensor measurements.

Statistical analyses. We examined a variety of metrics to characterize sub-daily and between-day variation. To quantify the underestimation in CO_2 emissions due to a daytime bias, we compared total CO_2 emissions estimated using hourly measurements with total emissions estimated from the average measurements between 10:00 and 14:00, the interquartile range of the observations in the GLORICH database. Given the non-normality of results among sites, we present uncertainty as normal bootstrapped intervals using the boot package (version 1.3-24) in R, with 10,000 replications. We quantified median CO_2 emissions (g C $m^{-2} d^{-1}$) during the day (between 12:00 and 17:00), median CO_2 emissions during the night (between 00:00 and 05:00), the absolute difference between day and night CO_2 emissions and the relative difference in CO_2 concentrations between day and night (in %; $((CO_{2,\,NIGHT} - CO_{2,\,DAY})/CO_{2,\,DAY}) \times 100$). Also, to evaluate differences between canopy levels we used the non-parametric Kruskal–Wallis test.

We explored temporal patterns of day–night CO_2 emission differences to test the influence of seasonality, local canopy cover and their interaction. We used piecewise SEM to evaluate causal and directional links between physical and biological parameters operating at the reach scale (Supplementary Table 2) and variance in daily day–night differences in CO_2 emissions. SEM is a theory-oriented multivariate statistical approach capable of testing a network of causal hypotheses by allowing evaluation of simultaneous influences rather than individual (bivariate) causes[50]. We first devised a metamodel (or metamodels) based on a priori theoretical knowledge and known mechanisms (see above; Fig. 3). The metamodel was fitted and tested using the function psem() in the piecewiseSEM R Package (version 2.1). To evaluate the effect sizes of each relationship (or path) within metamodels, the psem() model output provides estimates of individual (standardized) path coefficients (β). The evaluation of goodness of fit and associated uncertainty is performed through the coefficient of determination (R^2) and the residual standard error, respectively. Compared with traditional variance–covariance-based SEM, piecewise SEM allows for fitting of models to different distributions through a generalized linear model. SEM modelling was conducted using only summer data, which is when most of the sites are represented (Supplementary Fig. 1).

Data availability

Data are freely available at Zenodo (https://doi.org/10.5281/zenodo.4321623). Data can be explored interactively at: https://gmrocher.shinyapps.io/night_co2_emissions_streams/.

References

40. Guth, P. L. Drainage basin morphometry: a global snapshot from the shuttle radar topography mission. *Hydrol. Earth Syst. Sci.* **15**, 2091–2099 (2011).
41. Schneider, C. L. et al. Carbon dioxide (CO_2) fluxes from terrestrial and aquatic environments in a high-altitude tropical catchment. *J. Geophys. Res. Biogeosci.* **125**, e2020JG005844 (2020).
42. Rocher-Ros, G. et al. Metabolism overrides photo-oxidation in CO_2 dynamics of Arctic permafrost streams. *Limnol. Oceanogr.* https://doi.org/10.1002/lno.11564 (2020).
43. Dinsmore, K. J., Billett, M. F. & Dyson, K. E. Temperature and precipitation drive temporal variability in aquatic carbon and GHG concentrations and fluxes in a peatland catchment. *Glob. Change Biol.* **19**, 2133–2148 (2013).
44. Lynch, J. K., Beatty, C. M., Seidel, M. P., Jungst, L. J. & DeGrandpre, M. D. Controls of riverine CO_2 over an annual cycle determined using direct, high temporal resolution p_{CO_2} measurements. *J. Geophys. Res. Biogeosci.* **115**, G03016 (2010).
45. Teodoru, C. R. et al. Dynamics of greenhouse gases (CO_2, CH_4, N_2O) along the Zambezi River and major tributaries, and their importance in the riverine carbon budget. *Biogeosciences* **12**, 2431–2453 (2015).

46. Borges, A. V. et al. Variations in dissolved greenhouse gases (CO_2, CH_4, N_2O) in the Congo River network overwhelmingly driven by fluvial–wetland connectivity. *Biogeosciences* **16**, 3801–3834 (2019).
47. Le, T. P. Q. et al. CO_2 partial pressure and CO_2 emission along the lower Red River (Vietnam). *Biogeosciences* **15**, 4799–4814 (2018).
48. Olson, D. M. et al. Terrestrial ecoregions of the world: a new map of life on Earth: a new global map of terrestrial ecoregions provides an innovative tool for conserving biodiversity. *BioScience* **51**, 933–938 (2001).
49. Ulseth, A. J. et al. Distinct air–water gas exchange regimes in low- and high-energy streams. *Nat. Geosci.* **12**, 259–263 (2019).
50. Lapierre, J.-F., Guillemette, F., Berggren, M. & del Giorgio, P. A. Increases in terrestrially derived carbon stimulate organic carbon processing and CO_2 emissions in boreal aquatic ecosystems. *Nat. Commun.* **4**, 2972 (2013).

Acknowledgements

We thank S. Blackburn, J. Crawford, the Krycklan Catchment study and the Swedish Infrastructure for Ecosystem Science for sharing data used in this study. This study was largely supported by a Formas grant to R.A.S. Datasets provided by the StreamPULSE Network were funded by the National Science Foundation Macrosystems program (NSF Grant EF-1442439). D.A.R.-I. acknowledges support from the National Science Foundation (Grant EAR-1847331).

Author contributions

L.G.-G., G.R.-R. and R.A.S designed the study and wrote the paper with input from M.J.C. L.G.-G. and G.R.-R. compiled, processed and analysed the data. Å.H. provided remote sensing estimates. All authors contributed with data and commented on the earlier versions of this manuscript.

Competing interests

The authors declare no competing interests.

Additional information

Extended data is available for this paper at https://doi.org/10.1038/s41561-021-00722-3.

Supplementary information The online version contains supplementary material available at https://doi.org/10.1038/s41561-021-00722-3.

Correspondence and requests for materials should be addressed to L.G.-G. or G.R.-R.

Peer review information *Nature Geoscience* thanks Alberto Borges, Pierre Regnier and Jun Xu for their contribution to the peer review of this work. Primary Handling Editor: Xujia Jiang.

Reprints and permissions information is available at www.nature.com/reprints.

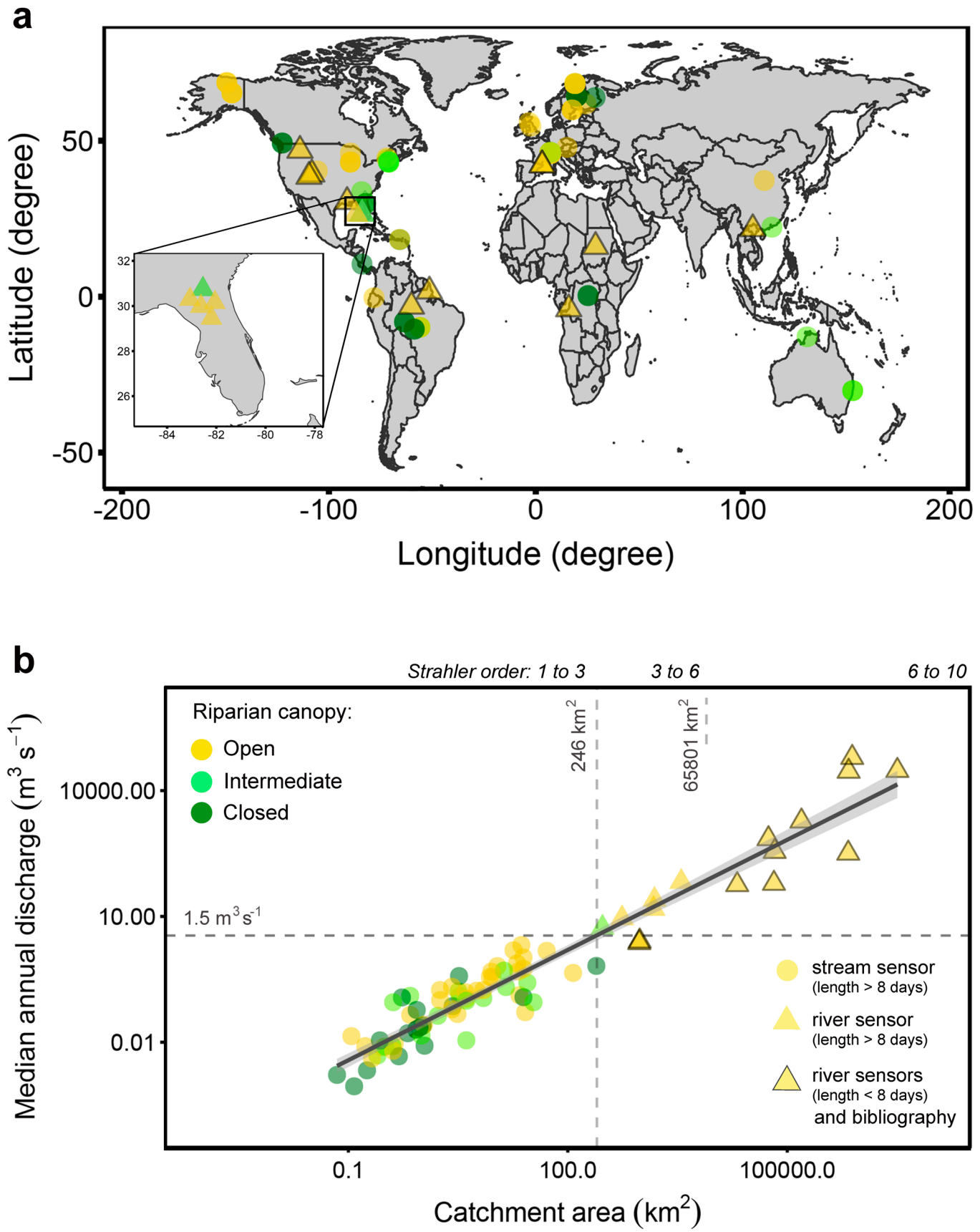

Extended Data Fig. 1 | Geographical and size distribution of the dataset. a) Global distribution of the stream and river sites colored by canopy cover category. **b)** Distribution and relationship between catchment area and median annual discharge, colored by canopy cover category. Symbols indicate the origin of the data (see Supplementary Table 1 and Supplementary Table 5 for more information).

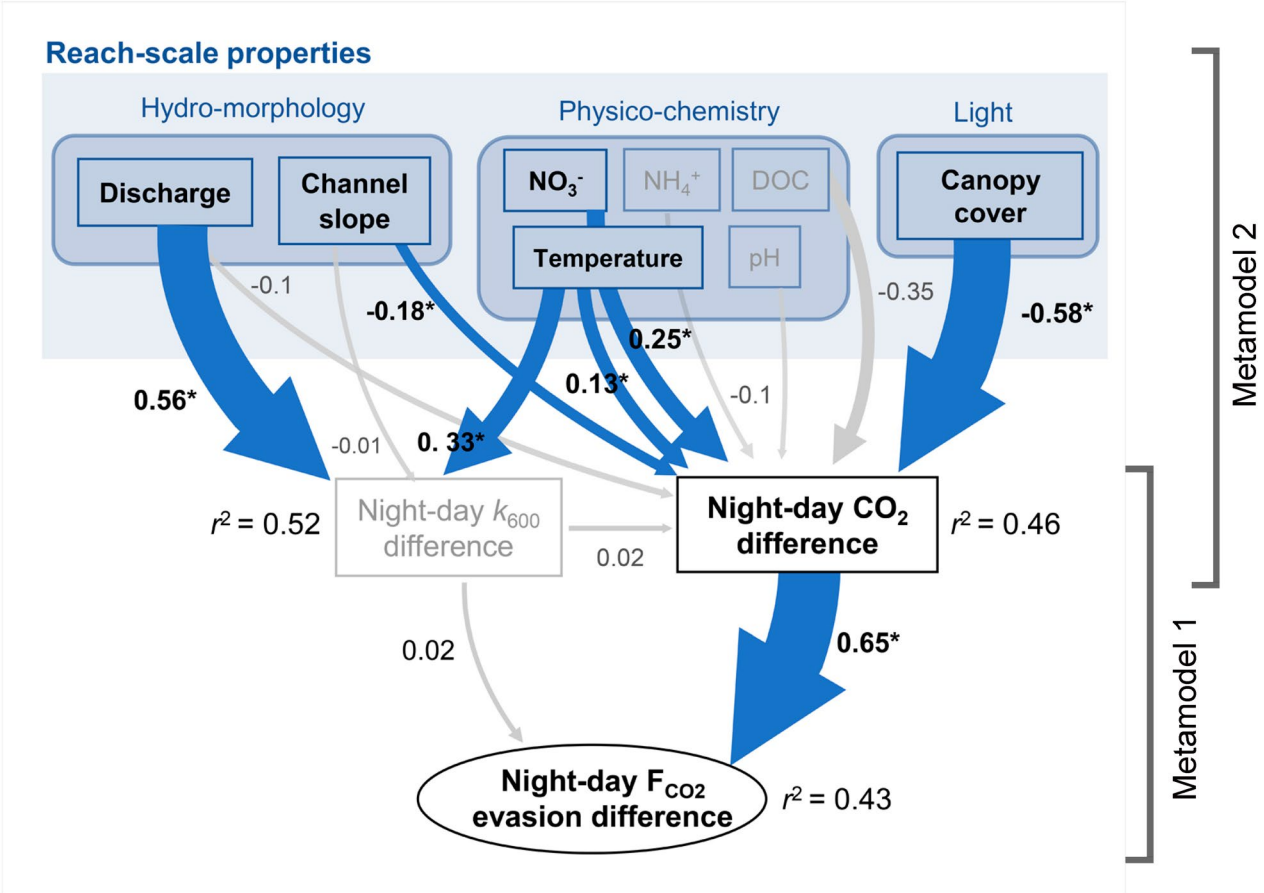

Extended Data Fig. 2 | Drivers of night-day differences of CO_2 emissions from streams. Structural equation model (SEM) representing connections between reach-scale physical and biological parameters contributing to the relative night-day variation in summertime CO_2 emissions (%). The SEM consisted of two dependent levels of factor interaction or metamodels. Metamodel 1 assessed the influence of kCO_2 and stream water pCO_2 on night-day differences of CO_2 emissions. Metamodel 2 assessed relationships between environmental variables and diel changes in stream water pCO_2. Blue arrows represent statistically significant effects ($p < 0.05$). Numbers adjacent to arrows are the standardized effect sizes of each relationship. Arrow width is proportional to the effect size. SEM goodness of fit was evaluated based on variance explained by each of the two models (r^2). A summary of statistical outputs from the SEM model is provided in Supplementary Table 4. Reach-scale properties for each site used in the SEM model are presented in Supplementary Table 2.

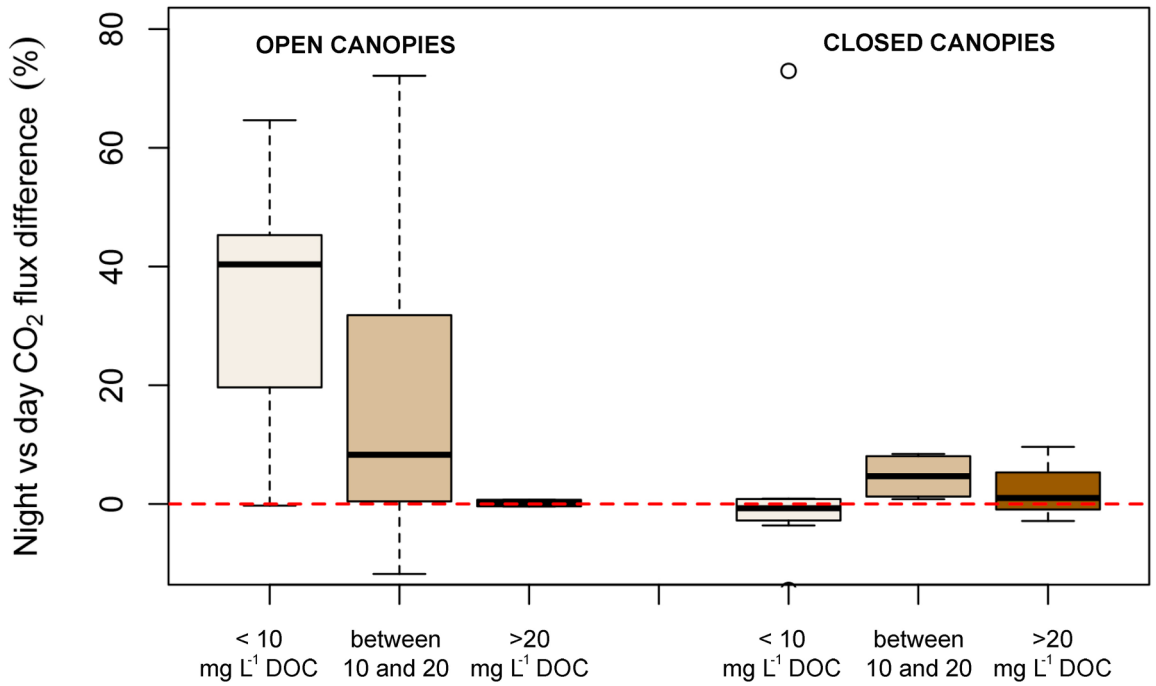

Extended Data Fig. 3 | Effect of water colour on the night-day differences in riverine CO_2 emission fluxes. Comparison of night-day differences in CO_2 emission fluxes averaged by watercourse and grouped by canopy level and dissolved organic carbon concentration (DOC; mg L^{-1}) level (lower than 10 mg L^{-1}, between 10 and 20 mg L^{-1}, and higher than 20 mg L^{-1}). Box plots display the 25th, 50th, and 75th percentiles whiskers display minimum and maximum values.

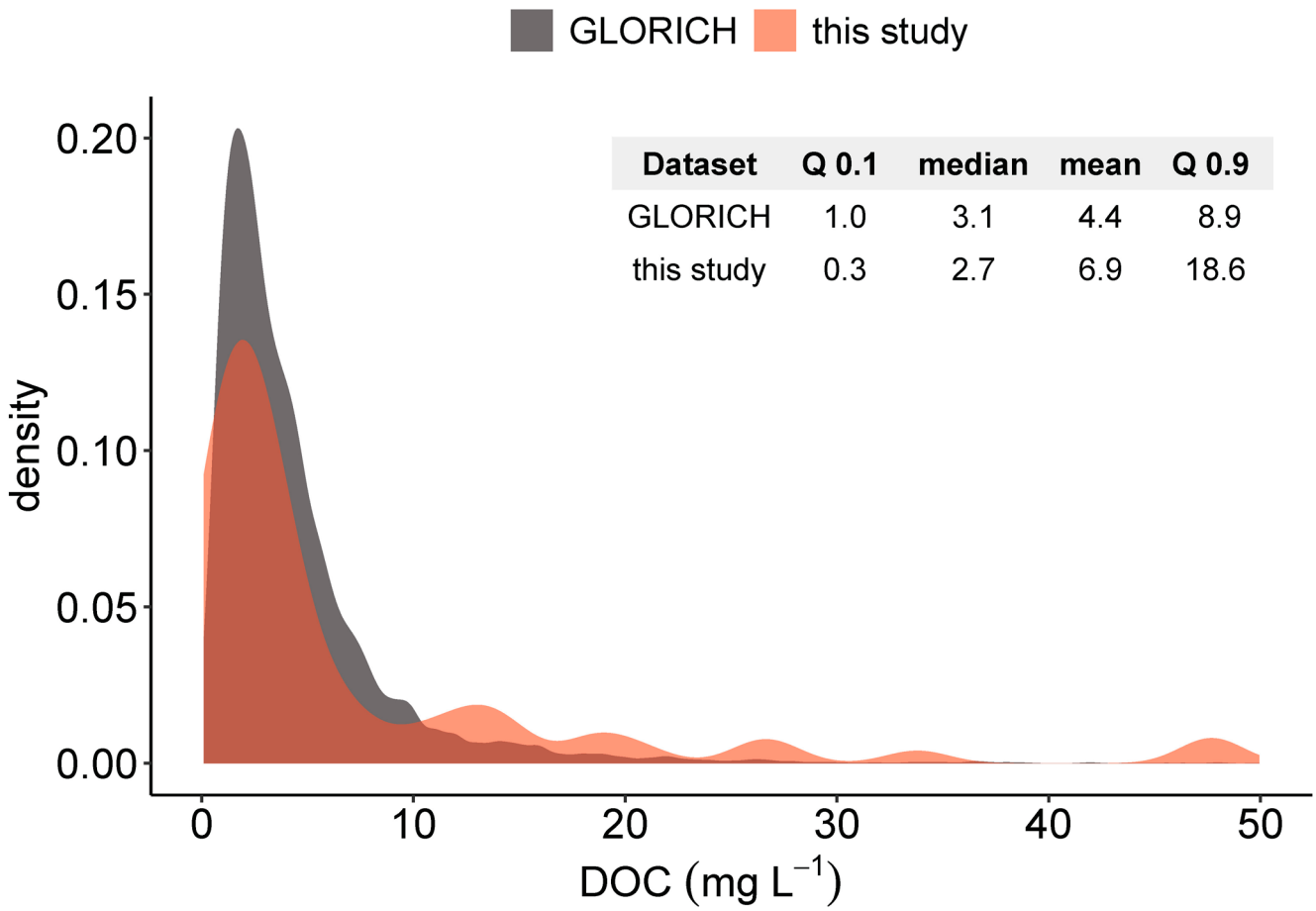

Dataset	Q 0.1	median	mean	Q 0.9
GLORICH	1.0	3.1	4.4	8.9
this study	0.3	2.7	6.9	18.6

Extended Data Fig. 4 | Distribution of dissolved organic carbon (DOC) in the GLORICH dataset and in this study. Inset table shows a selection of summary statistics. In the GLORICH database[12], 92.6 and 98.5 % of the samples were below 10 and 20 mg L^{-1} respectively. 15 observations from the GLORICH database (out of 6,771) had DOC > 50 mg L^{-1} and are not represented in the density plot for better visualization (max. value 839 mg L^{-1}).

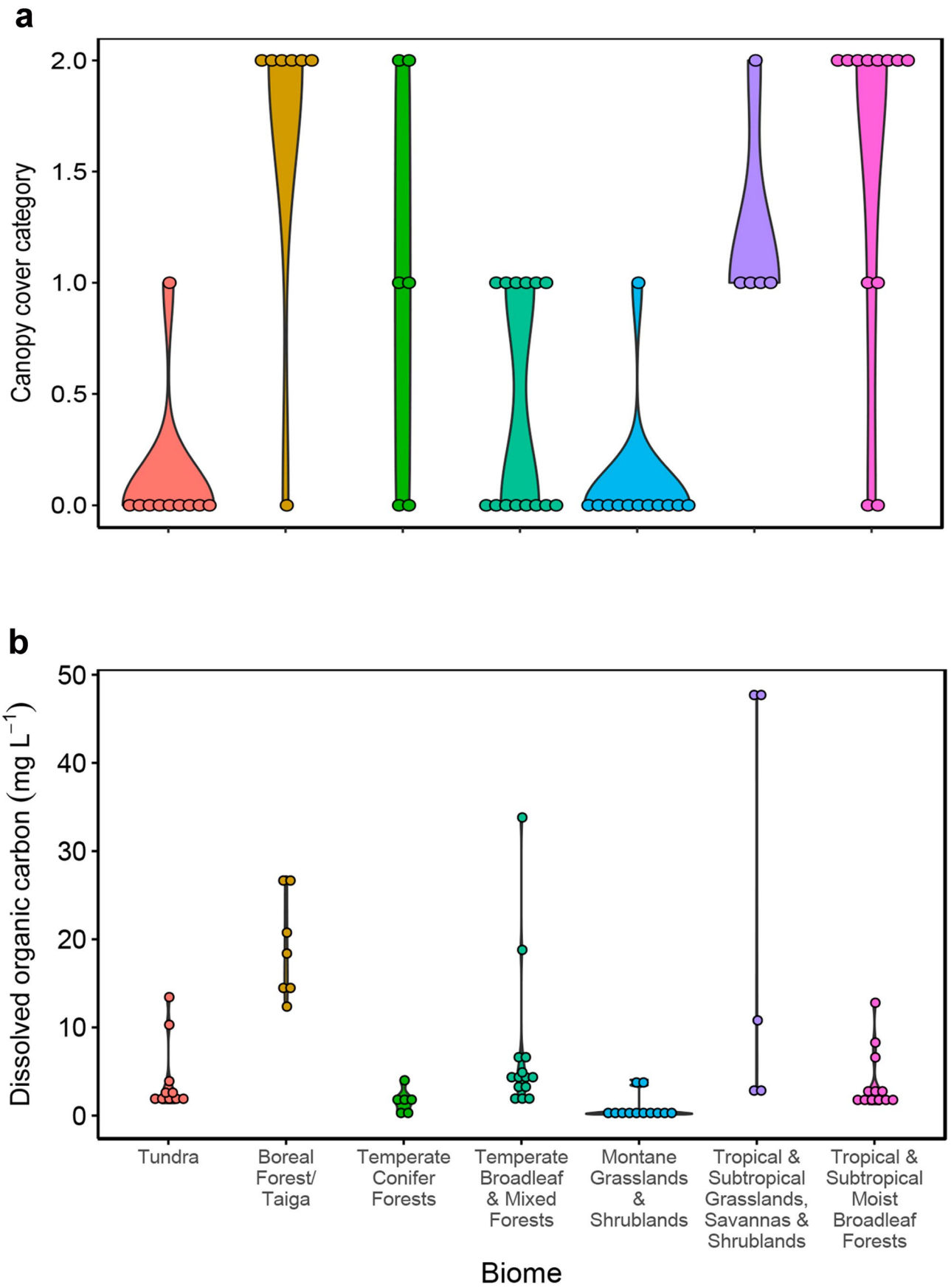

Extended Data Fig. 5 | Distribution of stream canopy cover and DOC concentrations by biome. Panel a shows the canopy cover distribution for each biome (note that canopy category can only be 0, 1 or 2). Panel b represents the ranges in DOC for each biome.